

Enhancement of ferroelectricity at metal/oxide interfaces

Massimiliano Stengel,¹ David Vanderbilt,² and Nicola A. Spaldin¹

¹*Materials Department, University of California, Santa Barbara, CA 93106-5050, USA*

²*Department of Physics and Astronomy, Rutgers University, Piscataway, New Jersey 08854-8019, USA*

(Dated: November 16, 2020)

By performing first-principles calculations on four capacitor structures based on BaTiO₃ and PbTiO₃, we determine the intrinsic interfacial effects that are responsible for the destabilization of the polar state in thin-film ferroelectric devices. We show that, contrary to the established interpretation, the interfacial capacitance depends crucially on the local chemical environment of the interface through the force constants of the metal-oxide bonds, and is not necessarily related to the bulk screening properties of the electrode material. In particular, in the case of interfaces between AO-terminated perovskites and simple metals, we demonstrate a novel mechanism of “interfacial ferroelectricity” that produces an overall *enhancement* of the ferroelectric instability of the film, rather than a suppression as is usually assumed. The resulting “negative dead layer” suggests a route to thin-film ferroelectric devices that are free of deleterious size effects.

PACS numbers: 71.15.-m, 77.84.-s, 73.61.Ng

Capacitors based on ferroelectric perovskites are potentially attractive for applications in nanoelectronics, such as non-volatile random-access memories and high-permittivity gate dielectrics. Thin-film geometries are sought after for optimal efficiency and information storage density [1]. However, in the thin-film regime, strong size-dependent effects arise. These can considerably worsen the attractive functionalities of the ferroelectric material by, e.g., reducing the dielectric response [2, 3] and causing rapid polarization relaxation [4]. Understanding and addressing these deleterious effects is crucial for future progress [5].

Several hypotheses have been formulated to interpret size effects in thin-film ferroelectric capacitors. Usually the experimental data can accurately be described in terms of the “series capacitor model,” where the overall capacitance density C of the device is written as

$$\frac{1}{C} = \frac{1}{C_1} + \frac{4\pi t}{\epsilon_b} + \frac{1}{C_2}. \quad (1)$$

Here ϵ_b is the bulk permittivity of the dielectric material of thickness t and $C_{1,2}$ are capacitances associated with low-permittivity layers located at the film/electrode interfaces. Such interfacial capacitances produce a depolarizing field [6, 7] that strongly reduces the dielectric response in the paraelectric regime and can destabilize the single-domain ferroelectric state. An accurate knowledge of the interfacial capacitance and its dependence on the combination of ferroelectric and electrode materials is, therefore, crucial for device design.

Interestingly, such interfacial “dead layers” are present even in high-quality epitaxial systems where the defect density is very low [4]. This suggests possible fundamental issues affecting the polarization at the metal/ferroelectric boundary. In particular, within the Thomas-Fermi model, many authors focus on the imperfect compensation of the polarization charges due to the finite electronic screening length of metallic electrodes.

To explain the substantially better performance of SRO electrodes as compared to Pt ones, as has been observed experimentally [2, 3], one can then invoke the lattice contribution to the screening, which is expected to be significant [8] in oxide electrodes.

The above interpretation, however, is clearly unsatisfactory at the microscopic level. The region where the interface effects occur is as thin as a few interatomic spacings [9]. In this region the local chemical and electrostatic environment departs significantly from that of either parent material, and a description of the interface in terms of bulk parameters is unjustified [5]. To describe such effects, a full quantum-mechanical treatment is required.

First-principles calculations have already been invaluable in understanding the properties of nanoscale ferroelectrics. Several studies have focused on the effects of strain [10, 11] and interfacial electrostatics [6, 12, 13] in determining the spontaneous polarization of symmetric [14] or asymmetric [15] capacitor geometries with various ferroelectric/electrode combinations. While most authors agree on the existence of a depolarizing field that tends to suppress single-domain ferroelectricity, a clear description of the microscopic mechanisms causing it has not yet emerged. Until it does, it will be difficult to overcome this deleterious behavior. The recent development of rigorous first-principles methods to define and control the polarization in a metal/ferroelectric heterostructure [16, 17] now provides the opportunity to perform such analysis.

In the present work we concentrate on ultrathin ferroelectric capacitor structures in which the ferroelectric is PbTiO₃ (PTO) or BaTiO₃ (BTO) and the metallic electrode can be SrRuO₃ (SRO) or Pt. Aside from being technologically relevant combinations, these are diverse enough to cover several kinds of behavior while remaining focused enough to allow an in-depth analysis. We find that the interfacial dielectric response is more complex

than usually assumed in phenomenological models, where only the penetration of the electric field in the electrode is considered. In particular, we develop a rigorous theory, based on the modern theory of polarization, in which the interface-specific effects of purely electronic screening and of interatomic force constants are both taken fully into account in assessing the overall performance of the capacitor. Based on our analysis, we demonstrate a covalent bonding mechanism that yields a *ferroelectric* behavior of the interface between AO-terminated films and simple metals. In this case one finds an overall *enhancement* of the driving force of the film towards a polar state, rather than a suppression as is predicted by semiclassical theories.

Our calculations are performed within the local-density approximation of density-functional theory and the projector-augmented-wave method [18] as implemented in an in-house code. An isolated capacitor with semi-infinite leads is modeled by a periodic array of alternating metallic and insulating layers, where the thicknesses of the metallic slab is treated as a convergence parameter and the ferroelectric film is N unit cells thick (the actual values are reported in Table I). We focus on symmetric interface terminations of the SrO/TiO₂ type for SRO electrodes, and of the Pt₂/AO type for Pt electrodes. In all cases we constrain the in-plane lattice parameter to the theoretical bulk SrTiO₃ value. We use our recently developed fixed- D [17] method, combined with the extensions to metal/insulator heterostructures of Refs. 16 and 19, to analyze the linear response of the paraelectric structure to a small polar perturbation. This regime is relevant for the existence of a (meta)stable single-domain ferroelectric state, and allows for a microscopic analysis of the physical ingredients contributing to the screening, without complications arising from asymmetries or pathological band alignments [5].

In order to assess the stability of a given structure against a polar distortion, we are concerned with C^{-1} , its inverse capacitance per in-plane unit cell, which can be expressed as [17]

$$C^{-1} = \left(\frac{4\pi}{S}\right)^2 \frac{d^2U}{dD^2} = -\frac{4\pi}{S} \frac{dV}{dD} \quad (2)$$

where U is the internal energy per in-plane cell, S is the cell area, and V is the potential drop across the capacitor plates. We note that C^{-1} is a “generalized” inverse capacitance that is meaningful even when it is negative [17], in which case it signals the appearance of an instability to a ferroelectric distortion in the capacitor arrangement – the more negative, the stronger the driving force towards a polar state.

We calculated C^{-1} for the four capacitor heterostructures considered in this work using a finite-difference approach. In particular, for each system we performed two complete electronic and structural relaxations, first at $D = 0$ by imposing a mirror symmetry, and then at

	N	$C^{-1}S$ (m ² /F)	$C_i^{-1}S$ (m ² /F)	N_{crit}	λ_{eff} (Å)
BTO/SRO	6.5	-1.553	2.280	4.85	0.202
PTO/SRO	6.5	0.439	1.727	7.45	0.153
STO/SRO	6.5	3.876	1.647	-	0.146
PTO/Pt	8.5	-1.427	1.258	5.42	0.111
BTO/Pt	8.5	-7.920	0.037	0.08	0.003

TABLE I: Calculated inverse capacitance densities $C^{-1}S$, interfacial inverse capacitance densities $C_i^{-1}S$, critical thickness N_{crit} and effective screening length λ_{eff} for the four capacitor heterostructures discussed in this work. Data for SRO/STO from Ref. 19 are reported for comparison.

$D = 0.001$ a.u. (a value that is small enough to ensure linearity) using our finite-field technique [16, 17]. This is possible because the fixed- D method allows one to define and compute the equilibrium state of an insulating system, within a given set of symmetry constraints and at a given value of macroscopic D , even in configurations that would be unstable at fixed electric field (e.g. a ferroelectric near the saddle point of its double-well potential). Finally, we extracted the induced bias potential and discretized Eq. (2) to obtain the inverse capacitances, whose values are reported in Table I. The positive sign of C^{-1} in the PTO/SRO case indicates that the system is paraelectric for the considered PTO thickness, while the other structures are in the ferroelectric regime.

A quantity that has received considerable attention in the recent past [6, 12, 13, 14] is the *critical thickness* for ferroelectricity, defined as the minimum thickness for which a polar state exists. The usual strategy to determine this quantity computationally is to perform several calculations for varying thicknesses until a spontaneous polarization appears. Instead, we find it much more convenient to exploit the power of the fixed- D approach and obtain such information directly from a calculation on a *single* thickness.

To that end, it is useful to look first at the spatial decomposition of the inverse capacitances shown in Fig. 1, where we plot the local inverse permittivity profiles $\epsilon^{-1}(x) = d\bar{\mathcal{E}}(x)/dD$ (evaluated at $D=0$), where $\bar{\mathcal{E}}$ is the x component of the y - z -averaged electric field along the stacking direction x . (These are calculated as in Ref. 19, except that our use here of the fixed- D method allows treatment of cases having $C^{-1} < 0$.) The profiles are generally characterized by two regions, an interfacial part where the imperfect screening manifests itself as a positive peak in $\epsilon^{-1}(x)$, and the deep interior of the insulating film where $\epsilon^{-1}(x)$ converges to the bulk value.

This naturally suggests a local decomposition between interface and bulk effects, where the overall stability of the centrosymmetric state emerges from the competition between these two usually opposite contributions. Rewriting Eq. (1) as $C^{-1} = C_1^{-1} + C_2^{-1} + NC_b^{-1}$, we

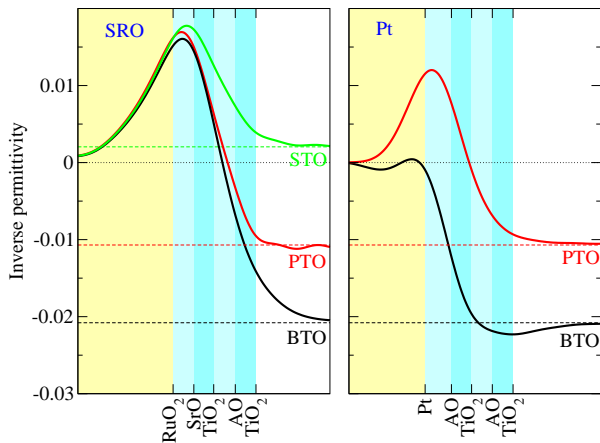


FIG. 1: Inverse local permittivity profiles for symmetric capacitor structures studied in this work. (For the SRO electrode, the STO curve from Ref. 19 is added for comparison.) Inverse permittivities calculated for bulk STO, BTO, and PTO are shown as dashed horizontal lines. Electrodes and oxide layers closest to the interface are indicated by shading.

obtain for a symmetric capacitor

$$C_i^{-1} = \frac{C^{-1} - NC_b^{-1}}{2}. \quad (3)$$

Here N is the number of bulk cells and $C_b^{-1} = 4\pi c_b / (\epsilon_b S)$ is the bulk inverse capacitance per unit cell (c_b is the cell parameter along the field direction). We take Eq. (3), based on a symmetric capacitor, to be our *definition* of the interfacial inverse capacitance. (Note that the definition depends on the precise convention for specifying N ; we adopt the convention that N is the nominal thickness as illustrated by the examples in Table I.) Then, given C_i^{-1} and C_b^{-1} , we again use Eq. (1) to *predict* the critical thickness

$$N_{\text{crit}} = -\frac{C_1^{-1} + C_2^{-1}}{C_b^{-1}} \quad (4)$$

for ferroelectricity in a (possibly asymmetric) capacitor, this being the value of N that yields an overall vanishing inverse capacitance. For an interface to a ferroelectric material ($C_b^{-1} < 0$), it is also natural to define the effective *dead-layer thickness* $N_{\text{dead},i} = -C_i^{-1}/C_b^{-1}$, in terms of which

$$N_{\text{crit}} = N_{\text{dead},1} + N_{\text{dead},2} \quad (5)$$

or, for a symmetric capacitor, $N_{\text{crit}} = 2N_{\text{dead}}$.

The calculated values for C_i^{-1} and N_{crit} are reported in Table I, together with the values already calculated in Ref. [19] for paraelectric SrTiO₃ (STO) between SRO electrodes. Since many authors discuss interfacial effects in terms of effective screening lengths $\lambda_{\text{eff}} = C_i^{-1}S/4\pi$

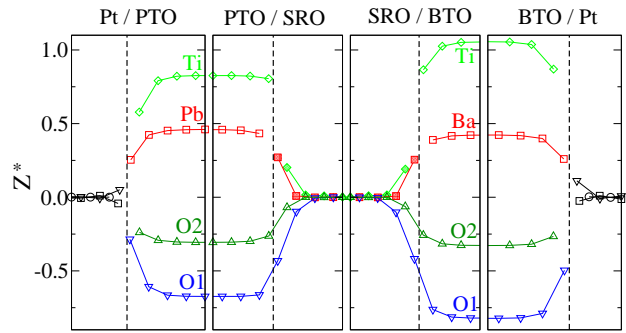


FIG. 2: Plots of Callen dynamical charges, arranged head-to-head and tail-to-tail to emphasize rapid convergence to common bulk values. Colored symbols denote A-site cations (red squares), B-site cations (light green diamonds), AO oxygens (O1, blue down triangles), and BO₂ oxygens (O2, dark green up triangles). The Pt atoms (black symbols) are labeled according to their projection onto the interface plane. Of the four independent Pt sites, one is shared with the A cations (squares), another is shared with O1 (down triangles) and the remaining two, equivalent by symmetry, are shared with O2 (circles).

rather than capacitances, we also report these values in the table.

It is rather surprising that the calculated N_{crit} of BTO/SRO is smaller than that of PTO/SRO. Indeed, PTO has a much larger spontaneous polarization P_s in the tetragonal ground state than BTO, and one would be tempted to think that the former is a “stronger” ferroelectric and therefore should have a smaller critical thickness. The calculated trend in N_{crit} is even more surprising on observing that C_i^{-1} of PTO/SRO is smaller than that of BTO/SRO, which would favor the opposite trend. It is clear from Eq. (4), however, that $|C_b^{-1}|$, rather than P_s , is the parameter that defines the strength of the bulk ferroelectric instability; at the fixed STO in-plane lattice constant, our calculated $|C_b^{-1}|$ is about twice as large in BTO than in PTO, which agrees nicely with the trend in N_{crit} . This highlights the fact that $|C_b^{-1}|$, rather than P_s , is the important parameter to consider when discussing the competition of bulk and interfacial electrostatics in ferroelectric capacitors.

In the Pt-based systems considered here, λ_{eff} is systematically smaller than in the SRO-based systems, in stark contrast with the predictions of the semiclassical models of Refs. 8, 20. (First-principles calculations have already demonstrated, in the case of STO paraelectric capacitors, that Pt electrodes can be intrinsically superior to SRO electrodes [19].) Here, while in PTO/Pt λ_{eff} is still significant, in the case of BTO/Pt it practically vanishes, or equivalently, the dead-layer thickness of $N_{\text{dead}} = 0.04$ layers is almost zero! This suggests that novel effects must take place at this interface that go be-

System	d (Å)	δ_{Pt} (Å)	δ_{AO} (Å)
BTO/Pt	2.26	0.46	0.12
PTO/Pt	2.11	0.34	0.19

TABLE II: Computed structural parameters for Pt₂-AO interfaces. See Fig. 3 for the definition of the symbols.

yond the usual Thomas-Fermi arguments, which always predict the same, positive value independent of the ferroelectric material.

To investigate the origin of such effects, we perform a microscopic analysis of the electrostatic response to a D field in the two Pt-based capacitors. The static inverse capacitance can be decomposed as

$$C^{-1} = (C^{\infty})^{-1} - \Delta \quad (6)$$

where $(C^{\infty})^{-1}$ is the purely electronic, frozen-ion value and $-\Delta$ is the lattice contribution. The latter can be expressed in terms of the Callen (or longitudinal) dynamical charge tensor Z^L [21], and the longitudinal force constant matrix \mathbf{K}^L , as

$$\Delta = \left(\frac{4\pi}{S}\right)^2 \sum_{ij} Z_{i,x}^L (K^L)_{ij}^{-1} Z_{j,x}^L \quad (7)$$

where x is again the stacking direction. Note that the sums in Eq. (7) run over *all* atoms in principle, including those located deep in the metallic electrodes, but in practice these do not contribute because their dynamical charges are zero (see Fig. 2). The convenience of using Eq. (7) instead of the usual decomposition involving transverse quantities, e.g. Eq. (8) of Ref. 22, is that, in a layered heterostructure, \mathbf{K}^L is *short-ranged* in real space [23, 24]. This means that local bonding effects can be unambiguously separated from the long-range electrostatic interactions, thus allowing for a detailed analysis of the microscopic mechanisms contributing to the polarization.

It is clear from Eq. (7) that two basic ingredients contribute to the ionic polarizability, the force constants contained in \mathbf{K}^L , and the dynamical charge associated with a given degree of freedom, Z^L . Since the *inverse* of \mathbf{K}^L enters the sum, it is obvious that *less stable* bonds will yield an enhanced response, provided that the participating atoms carry a significant Z^L . It is reasonable then to expect that the relative weakness of the bonds formed by the ferroelectric films with Pt, compared to those formed with the isostructural conducting oxide SRO, might explain the enhanced interfacial dielectric properties of the former electrode material, and might also help shed some light on the qualitatively different behavior of PTO/Pt and BTO/Pt.

To investigate this hypothesis, we start by looking at the relaxed geometry of the interfacial Pt₂ and AO lay-

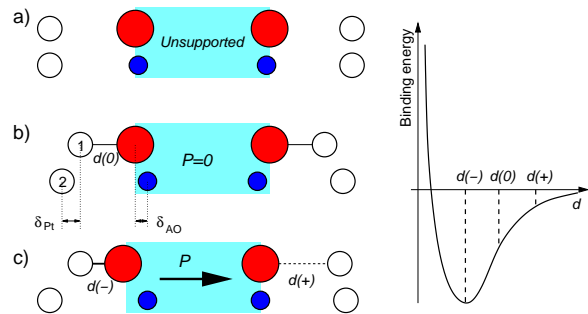


FIG. 3: Schematic representation of the salient features of the Pt₂-AO interface. Only interfacial atoms are shown; empty, red, and blue circles denote Pt, O, and A atoms respectively. (a) Unsupported film and metal surfaces. A small surface rumpling is present only in the AO surface layer while the metal is flat. (b) Centrosymmetric interface geometry, with significant rumplings δ , especially in the Pt₂ layer. (c) Proposed mechanism for interfacial ferroelectricity, driven by the unstable Pt-O bond. Right: example of a two-body binding energy curve having negative curvature at $d(0)$.

ers when the film is in the centrosymmetric configuration, schematically shown in Fig. 3. The significant rumpling δ which is present in both Pt₂ and AO (values are reported in Tab. II) brings Pt(1) and the interface O atoms in much closer contact than the neighboring Pt(2) and A cation, indicating that only the former two atoms form a true chemical bond. Moreover, the strong buckling in the Pt₂ layer is indicative of a frustrated bonding environment, where the repulsive A-Pt interaction is in competition with the attractive O-Pt bond. As a result, the O-Pt distance d in the relaxed interface structures is in both cases significantly larger than the typical Pt-O equilibrium distance of about 2.0 Å, which has been determined experimentally and theoretically in a number of bulk oxide phases [25]. Comparing the interface systems, d is even larger in BTO/Pt than in PTO/Pt, indicating that the Pt-O bond is weaker in the former system.

To quantify this difference in strength, we examine the local force constants characterizing the Pt-O interfacial bond. At the PTO/Pt interface we have $K_{\text{Pt-O}}^L = -0.039$ a.u., which is comparable to the typical interatomic force constants in oxide crystals and is consistent with a *stable* chemical bond. Strikingly, at the BTO/Pt interface we have $K_{\text{Pt-O}}^L = 0.001$ a.u., a very small and positive value, which indicates that the Pt-O bond here is slightly *unstable* (i.e. there is no restoring force associated to it). This indicates that the structural frustration present at the interface is strong enough in BTO/Pt to pull the Pt-O bond into an unstable regime [see Fig. 3 (right)]. This qualitative difference between PTO/Pt and BTO/Pt is entirely responsible for their inequivalent polar response, as we shall see in the following.

In order to link the stability of the Pt(1)-O bond to the dielectric response of the capacitor, we perform a

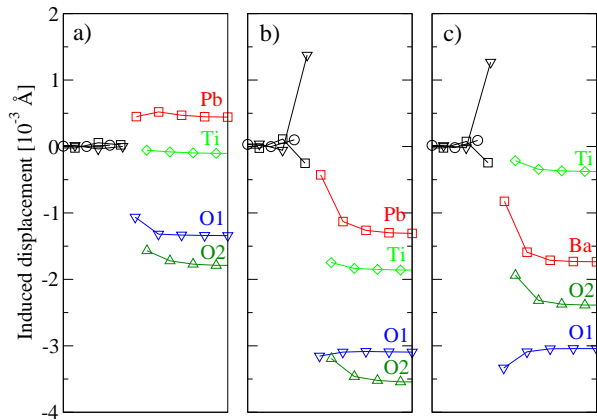


FIG. 4: Ionic displacements induced by a small field of $D = 10^{-3}$ a.u. ($0.455 \mu\text{C}/\text{cm}^2$). (a) PTO/Pt; (b) PTO/Pt modified by artificial addition of force constant $k = -0.05$ a.u.; (c) BTO/Pt. The color/symbol scheme is the same as in Fig. 2. The horizontal axis is the x coordinate, normal to the interface plane, and refers to the relaxed atomic positions in the centrosymmetric geometry.

computational experiment in which we artificially modify the force constant matrices \mathbf{K}^L of PTO/Pt and BTO/Pt by adding a negative harmonic term of the form $E_h = (k/2)[x_O - x_{\text{Pt}} - d(0)]^2$ between Pt(1) and O, which weakens the corresponding bond without changing the centrosymmetric equilibrium geometry. Our goal is to demonstrate that, by choosing an appropriate value of k , one can destabilize the Pt(1)-O bond at the PTO/Pt interface and therefore reproduce the behavior (dead-layer thickness and atomic displacement pattern) of the BTO/Pt system. To that end, we choose $k = -0.05$ a.u. (a value slightly larger than $K_{\text{Pt-O}}^L$) and we recalculate the effective dead-layer thickness for PTO/Pt by inserting this modified \mathbf{K}^L matrix into Eq. (7). Remarkably, due to the additional harmonic term E_h , $N_{\text{dead}} = 2.71$ jumps to a very small value $N_{\text{dead}} = 0.08$, practically identical to that of the unmodified BTO/Pt case.

To further prove that the “modified” PTO/Pt behaves in all important respects like BTO/Pt, we plot in Fig. 4 the induced ionic displacements in three different cases: PTO/Pt ($k = 0$), PTO/Pt ($k = -0.05$), and BTO/Pt ($k = 0$). Note that the ionic responses to a small D field are very different in the first and last cases. In this context, it is remarkable that the middle “modified PTO/Pt” case is strikingly similar to BTO/Pt, even in many fine details of the induced relaxations at the interface layers. Deeper into the oxide, the displacements reflect the different ferroelectric mode patterns (e.g., there is a larger displacement for Pb than for Ba because of the stereochemical activity of the Pb lone pairs), but the behavior of the first oxide layers is nearly identical. This unambiguously demonstrates that the dissimilar behav-

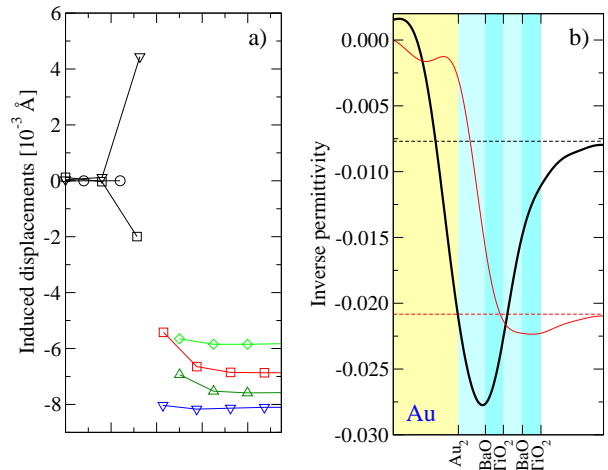


FIG. 5: Computed local properties at the BTO/Au interface. (a) Ionic displacements induced by a small field of $D = 0.001$ a.u.; (b) Inverse permittivity profile (thick solid black curve) compared with corresponding BTO/PT results (thin solid red curve) as in Fig. 1. The thin dashed lines in (b) indicate the values of the bulk inverse permittivity of BTO at $D = 0$ for two different values of the in-plane strain, 0% (black) and -2.2% (black), corresponding to the cubic lattice constants of BTO and STO, respectively.

ior in the BTO/Pt and PTO/Pt cases is almost entirely due to the change in stability of the Pt-O bond.

Now, to have a mechanism for ferroelectricity, a structural instability needs to be coupled to the polarization. Comparing the original and the “modified” PTO/Pt ionic displacement patterns in Fig. 4(a) and (b), it is apparent that the stretching of the Pt-O bond is associated with i) a shift of the whole ferroelectric slab in the opposite direction to D , and ii) with a combined rumpling of the AO and Pt₂ layers. Since the atoms in both Pt₂ and AO carry significant values of Z^L (see Fig. 2), both effects have a strong impact on the polarization. We therefore identify this mechanism as a novel form of “interfacial ferroelectricity.” Here we have a flagrant breakdown of phenomenological models based on bulk properties of the parent materials.

These arguments lead to a quite general prediction, namely that AO-terminated perovskite ferroelectrics can show a strong interfacial enhancement of the ferroelectric properties when weakly bonded to a simple metal. To test this prediction, we performed a supplementary calculation for a BTO-based capacitor by replacing the Pt electrodes with a more inert material, Au. In this case the equilibrium lattice constant of bulk BTO was used for the epitaxial strain constraint, to better match the experimental setup of Ref. [26], but otherwise all computational parameters were kept the same. As before, we first relaxed the centrosymmetric geometry and then calculated the ionic and electronic response to a small field. The calculated induced ionic displacements for BTO/Au,

presented in Fig. 5(a), show the same qualitative features i) and ii) discussed above, but their magnitude is about four times larger than in BTO/Pt, reflecting the weaker Au-oxide interaction. Consistent with the enhanced displacements, we obtain a *negative dead-layer thickness* of $N_{\text{dead}} = -5.5$ layers, which manifests itself as an unusually large dip in the local permittivity profile, shown in Fig. 5(b). (Note the rather dissimilar bulk “ferroelectric strength” of BTO at the different in-plane strain states.) In other words, the actual capacitor with 8.5 layers of BTO and real Au electrodes has the same degree of ferroelectric instability as ~ 19.5 layers of BTO between “ideal” electrodes! It is quite remarkable that such a huge effect can be caused by only two atomic monolayers at the interface (Au₂ and BaO).

In conclusion, we have used a rigorous finite-field approach to study the influence of the electrode-film interface on the ferroelectric instability of nanoscale BaTiO₃ and PbTiO₃ capacitors. At the AO-terminated interfaces with simple metals, we demonstrate a strong correlation of the overall ferroelectric response of the capacitor to the strength of the interfacial metal-oxygen bond. In cases where this bond is especially weak, such as the BaO-Au interface, we find an unusually large enhancement of the ferroelectric instability. This result is in striking contrast with the conclusions of the Thomas-Fermi screening model, demonstrating that a microscopic analysis is generally necessary to describe interfacial effects in ferroelectric capacitors. This mechanism also suggests a possible route to the fabrication of nanoscale devices free from interfacial size effects.

Methods

Our calculations are performed within the local-density approximation of density-functional theory and the projector-augmented-wave method [18], with a planewave basis cutoff energy of 40 Ry. We constrain the in-plane lattice constant to the calculated theoretical equilibrium value for cubic SrTiO₃ ($a = 7.276$ a.u.) unless otherwise specified. We set the thickness of the insulating film to N unit cells (the actual values are reported in Table I). The thickness of the metal electrode slab was 7.5 unit cells of SRO or 11 atomic layers of Pt, which were sufficient to converge the interface properties of interest. We use a 6×6 Monkhorst-Pack sampling of the surface Brillouin zone, which reduces to 6 special points within the tetragonal symmetry. A Gaussian smearing of 0.15 eV was used to accelerate convergence of the Brillouin-zone integrations. We carefully checked that the band alignment at the interface and the choice of the smearing scheme is such that any spurious population of the conduction band of the insulating film is avoided. All the structural degrees of freedom were fully relaxed subject to the translational and point symme-

tries (a mirror symmetry plane is first imposed to relax the geometry in the paraelectric state, and later relaxed when calculating the linear response to a displacement field).

The insulating character of the system along the stacking direction (the insulator is thick enough so that direct tunneling is suppressed) allows for a rigorous definition of the macroscopic polarization and its coupling to an external bias voltage [16, 19]. Because at the quantum-mechanical level all wavefunctions are mutually coupled and there is no clear way to separate free conduction charge from the bound polarization charge we adopt the convention of treating *all* charges as bound charges, so that D is a constant throughout the heterostructure [27] just as for a purely insulating system [28]. What would customarily be called the macroscopic free charge σ on the top of the electrode is here reinterpreted as a bound charge associated with a polarization $P = \sigma$ in the metallic region. (Indeed $D = 4\pi\sigma$, since the electric field must vanish in the metallic region.)

All quantities requiring a derivative with respect to D were performed by finite differences between a calculation with mirror symmetry imposed ($D = 0$) and a fixed- D calculation with $D = 0.001$ a.u. The longitudinal force constant matrices and the dynamical charges were computed by finite differences by taking displacements of 0.4 mÅ along the tetragonal axis.

Acknowledgements

This work was supported by the Department of Energy SciDac program on Quantum Simulations of Materials and Nanostructures, grant number DE-FC02-06ER25794 (M.S. and N.S.), and by ONR grant N00014-05-1-0054 (D.V.).

-
- [1] Dawber, M., Rabe, K. M. & Scott, J. F. Physics of thin-film ferroelectric oxides. *Rev. Mod. Phys.* **77**, 1083 (2005).
 - [2] Hwang, C. S. Thickness-dependent dielectric constant of (Ba,Sr)TiO₃ thin films with Pt or conducting oxide electrodes. *J. Appl. Phys.* **92**, 432 (2002).
 - [3] Plonka, R., Dittmann, R., Pertsev, N. A., Vasco, E. & Waser, R. Impact of the top-electrode material on the permittivity of single-crystalline Ba_{0.7}Sr_{0.3}TiO₃ thin films. *Appl. Phys. Lett.* **86**, 202908 (2005).
 - [4] Kim, D. J. *et al.* Polarization relaxation induced by a depolarization field in ultrathin ferroelectric BaTiO₃ capacitors. *Phys. Rev. Lett.* **95**, 237602 (2005).
 - [5] Junquera, J. & Ghosez, P. First-principles study of ferroelectric oxide epitaxial thin films and superlattices: role of the mechanical and electrical boundary conditions. *arXiv:0711.4201* (2007).

- [6] Junquera, J. & Ghosez, P. Critical thickness for ferroelectricity in perovskite ultrathin films. *Nature* **422**, 506–509 (2003).
- [7] Pertsev, N. A., Dittmann, R., Plonka, R. & Waser, R. Thickness dependence of the intrinsic dielectric response and apparent interfacial capacitance in ferroelectric thin films. *J. Appl. Phys.* **86**, 202908 (2005).
- [8] Black, C. T. & Welser, J. J. Electric-field penetration into metals: Consequences for high-dielectric constant capacitors. *IEEE Trans. Electron Devices* **46**, 776 (1999).
- [9] Tagantsev, A. K. & Gerra, G. Interface-induced phenomena in polarization response of ferroelectric thin films. *J. Appl. Phys.* **100**, 051607 (2006).
- [10] Rabe, K. M. Theoretical investigations of epitaxial strain effects in ferroelectric oxide thin films and superlattices. *Curr. Opin. Solid State Mat. Sci.* **9**, 122 (2005).
- [11] Ederer, C. & Spaldin, N. A. Effect of epitaxial strain on the spontaneous polarization of thin film ferroelectrics. *Phys. Rev. Lett.* **95**, 257601 (2005).
- [12] Sai, N., Kolpak, A. M. & Rappe, A. M. Ferroelectricity in ultrathin perovskite films. *Phys. Rev. B* **72**, 020101(R) (2005).
- [13] Umeno, Y., Meyer, B., Elsässer, C. & Gumbsch, P. Ab initio study of the critical thickness for ferroelectricity in ultrathin Pt/PbTiO₃/Pt films. *Phys. Rev. B* **74**, 060101(R) (2006).
- [14] Gerra, G., Tagantsev, A. K., Setter, N. & Parlinski, K. Ionic polarizability of conductive metal oxides and critical thickness for ferroelectricity in BaTiO₃. *Phys. Rev. Lett.* **96**, 107603 (2006).
- [15] Gerra, G., Tagantsev, A. K. & Setter, N. Ferroelectricity in asymmetric metal-ferroelectric-metal heterostructures: A combined first-principles–phenomenological approach. *Phys. Rev. Lett.* **98**, 207601 (2007).
- [16] Stengel, M. & Spaldin, N. A. Ab-initio theory of metal-insulator interfaces in a finite electric field. *Phys. Rev. B* **75**, 205121 (2007).
- [17] Stengel, M., Spaldin, N. A. & Vanderbilt, D. Electric displacement as the fundamental variable in electronic-structure calculations. *arXiv:0806.0844* (2008).
- [18] Blöchl, P. E. Projector augmented-wave method. *Phys. Rev. B* **50**, 17953–17979 (1994).
- [19] Stengel, M. & Spaldin, N. A. Origin of the dielectric dead layer in nanoscale capacitors. *Nature* **443**, 679 (2006).
- [20] Choi, W. S. *et al.* Dielectric constants of Ir, Ru, Pt, and IrO₂: Contributions from bound charges. *Phys. Rev. B* **74**, 205117 (2006).
- [21] Ghosez, P., Michenaud, J.-P. & Gonze, X. Dynamical atomic charges: The case of ABO₃ compounds. *Phys. Rev. B* **58**, 6224–6239 (1998).
- [22] Antons, A., Neaton, J. B., Rabe, K. M. & Vanderbilt, D. Tunability of the dielectric response of epitaxially strained SrTiO₃ from first-principles. *Phys. Rev. B* **71**, 024102 (2005).
- [23] Giustino, F. & Pasquarello, A. Infrared spectra at surfaces and interfaces from first principles: Evolution of the spectra across the Si(100)-SiO₂ interface. *Phys. Rev. Lett.* **95**, 187402 (2005).
- [24] Wu, X., Stengel, M., Rabe, K. M. & Vanderbilt, D. Predicting polarization and nonlinear dielectric response of arbitrary perovskite superlattice sequences. *Phys. Rev. Lett.* **101**, 087601 (2008).
- [25] Seriani, N., Jin, Z., Pompe, W. & Colombi Ciacchi, L. Density functional theory study of platinum oxides: From infinite crystals to nanoscopic particles. *Phys. Rev. B* **76**, 155421 (2007).
- [26] Saad, M. M. *et al.* Intrinsic dielectric response in ferroelectric nano-capacitors. *J. Phys.: Condens. Matter* **16**, L451 (2004).
- [27] Strictly speaking, D and P here are the longitudinal components of the respective fields.
- [28] Giustino, F. & Pasquarello, A. Theory of atomic-scale dielectric permittivity at insulator interfaces. *Phys. Rev. B* **71**, 144104 (2005).